

Supplementary Information for

Non-linear Phase Linking using joined Distributed and Persistent Scatterers

Sara Mirzaee^{a,*}, Falk Amelung^a, Heresh Fattah^b

^a Rosenstiel School of Marine and Atmospheric Science, University of Miami, Miami, Florida, USA

^b Jet Propulsion Laboratory, California Institute of Technology, Pasadena, California, USA

*Correspondence to S. Mirzaee, sara.mirzaee@rsmas.miami.edu

Content of this file

Section S1. Coherence matrix simulation with supplemental Table S1

Section S2. Unwrapping error propagation with supplemental Figure S2.1 to S2.7 and Tables S2.1 to S2.3

Section S3. Additional information to section 6 with supplemental Figures S3.1 to S3.12 and Table S3.

Section S4. Technical software guide with Table S4.

Supplemental references.

Introduction

This supplement contains 4 sections. The first section contains the parameters for coherence matrix simulation (Section S1). The second section consists of the unwrapping networks and additional information for simulation of error propagation and another example for agricultural fields in Sicily, Italy, for varying unwrapping error propagation as a function of the unwrapping network (Section S2). The third section

contains additional information regarding applications in section 6 of the main paper (Section S3) and it includes the source of bias observed in classic small baseline approach and additional examples of construction-induced subsidence on Miami Beach island. The last section provides technical information about the MiaplPy software and describes the functionality of the standalone scripts and also discusses about the computational considerations (Section S4).

S1. Coherence matrix simulation

The model parameters for coherence matrix simulation are listed in Table S1. Refer to section 3 for the full explanation of the parameters.

Table S1: Model parameters for coherence matrix simulation (see Figure 1)

Temporal coherence model	Model parameters (A and B are the calculated seasonal decorrelation parameters)					
	τ (days)	v (mm/yr)	γ^0	γ^∞	A_s	B_s
Long-term coherent (Figure 1b)	50	4	0.6	0.1	n/a	n/a
Long-term decorrelated (Figure 1c)			0	n/a	n/a	
Light seasonal decorrelation (Figure 1d)			0.1	0.387	0.387	
Strong seasonal decorrelation (Figure 1e)			0	0.545	0.229	

S2. Unwrapping error propagation

In the first subsection of this section, we show the unwrapping networks used for simulation in section 4 (Section S2A). In the second subsection we show simulations for inversion of different unwrapping networks with L1- and L2-norm minimization assuming a non-zero displacement with random tropospheric artifacts (Section S2B). In the third subsection we show the RMSE, and velocity estimated for 1000 realization of simulated zero displacement time series for different networks (Section S2C). In the fourth subsection we

show the difference of displacements obtained from different networks with the one obtained from a single reference network (Section S2D). In the last subsection we show an example of unwrapping error propagation over agricultural fields after phase linking (Section S2E).

S2A Unwrapping networks

As we mentioned in section 4 in the main paper, we simulate different networks (Figure S2.1) to assess the unwrapping error propagation and we use the real baselines of Sentinel-1 data for two consecutive years. In the single reference network, we select the middle image as the reference image. For the Delaunay network, we use a scale factor of 4 for the ratio of perpendicular baselines to temporal baselines. For annual ministacks, we connect ministacks with three connections, one is between the reference images of the two ministacks, one is the smallest temporal baseline which is between the last image of the first ministack and first image of the second ministack, and the last one is a small perpendicular baseline between the two ministacks. For sequential networks, we select 3, 5 and 8 connections for comparison.

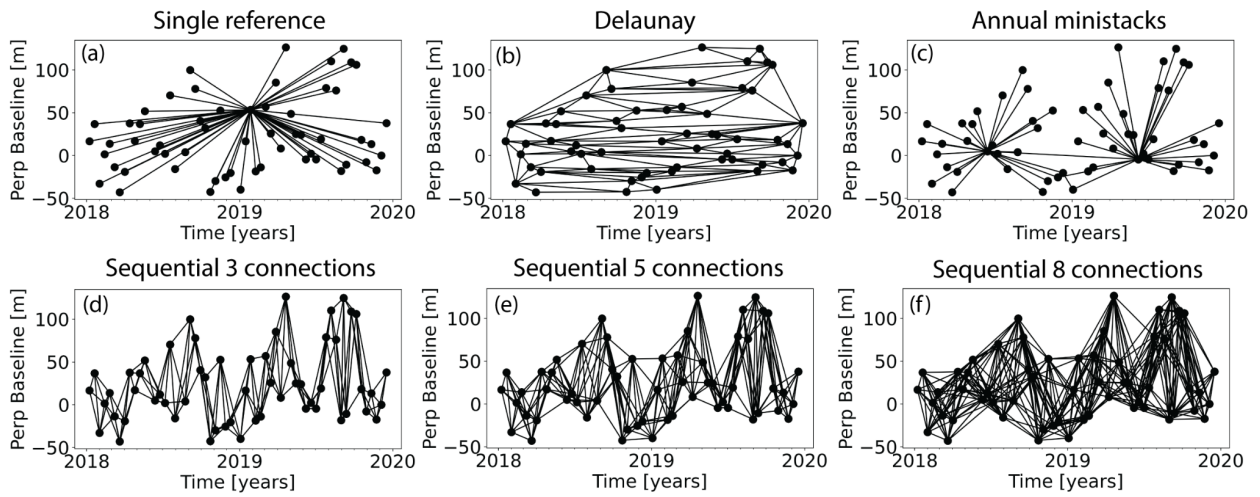


Figure S2.1: Interferogram networks for the simulation of the propagation of unwrapping errors. (a) Single reference network. (b) Delaunay network, (c) annual ministacks network, (d) sequential network with 3 connections, (e) sequential network with 5 connections, (f) sequential network with 8 connections.

S2B Non-zero displacement with tropospheric perturbations

We show the L1 and L2 norm inversion results for different unwrapping networks by simulating a non-zero displacement signal (4 cm/yr) with random tropospheric artifacts in time in the range of -0.5 to 0.5 cm in Figure S2.2. The results are consistent with our observations of zero displacement simulated data (section 4 in main paper).

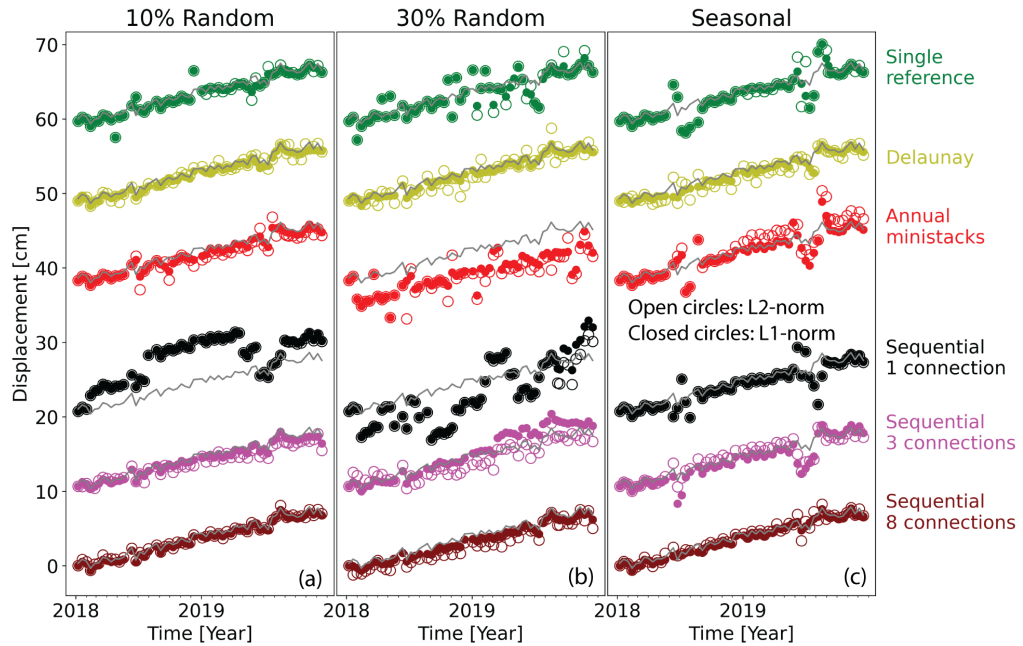


Figure S2.2: Similar to Figure. 3 but with a non-zero displacement and random variations in time as tropospheric contributions. Solid line is the simulated non-zero velocity time series.

S2C Statistical analysis of unwrapping networks

The histograms of the RMSE obtained from estimated time series of different unwrapping networks simulated with zero displacement after 1000 realizations is illustrated in Figure S2.3. The calculated median and median absolute deviation (MAD) are shown in Table S2.1 ($\text{median} \pm \text{MAD}$) (Refer to section 4 of the main paper for discussion).

To quantify the precision and accuracy of the estimated time series obtained from inverting different networks, we calculate the velocity of displacement with a linear regression for the above-mentioned

scenarios with 1000 realizations and compute median and median absolute deviations (Figure S2.4 and Table S2.2). The histograms of the estimated velocities obtained from Delaunay network illustrate a unimodal distribution with median and median absolute deviation close to zero for all scenarios (e.g., $0.00 \pm /- 0.10 \text{ cm/yr}$ for seasonal unwrap error inverted with L1 norm minimization). All other networks show a multimodal distribution and large median absolute deviations (up to 1.35 cm/yr) for seasonal unwrap errors. For random unwrap errors, the median absolute deviation decreases with more connections in sequential networks. The observations of the displacement velocities are consistent with the RMSE suggesting the Delaunay network as an accurate and precise estimation; however, the precision depends on the number of unwrapping errors.

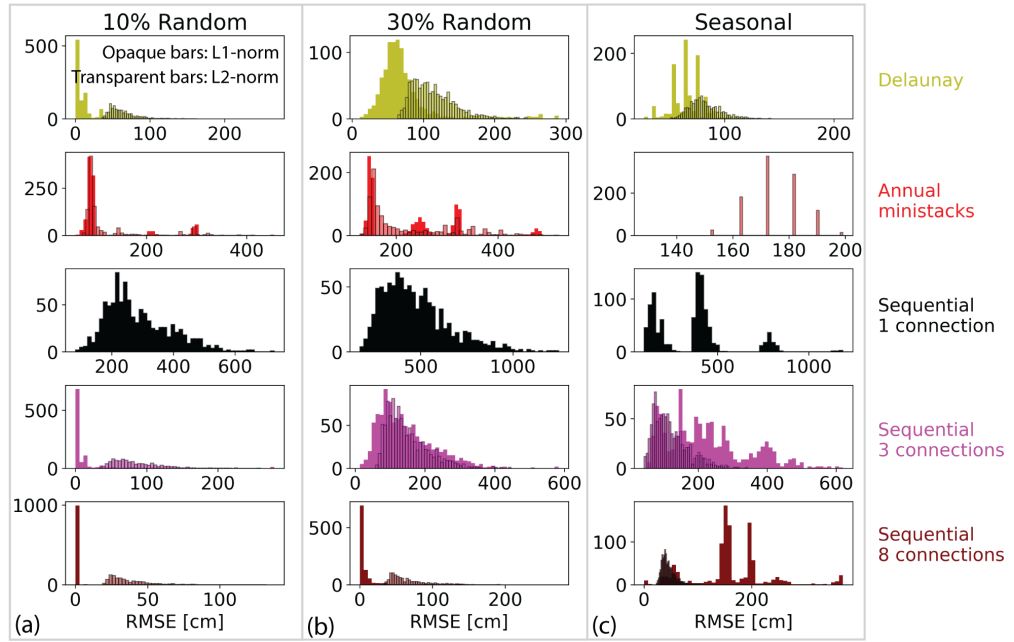


Figure S2.3: Histograms of the RMSE of the estimated time series obtained from inverting different simulated unwrapping networks after 1000 realizations. The unwrapping errors are similar to Figure 3 in 3 panels (a) 10% random unwrap errors, (b) 30% rundown unwrap errors, (c) seasonal unwrap errors (during 3 months period).

Table S2.1: Median and median absolute deviation of the RMSE of the time series obtained from simulating different unwrapping networks with 1000 realizations. Histograms shown in Figure S2.3

Unwrapping network	10% Random (cm)		30% Random (cm)		Seasonal (cm)	
	L1	L2	L1	L2	L1	L2
Delaunay	0.05 ± 0.05	0.58 ± 0.10	0.63 ± 0.13	1.06 ± 0.17	0.64 ± 0.10	0.80 ± 0.09
Annual ministacks	0.86 ± 0.05	0.91 ± 0.04	1.57 ± 0.18	1.73 ± 0.22	1.28 ± 0.00	1.73 ± 0.09
Sequential 1 connection	2.60 ± 0.63	2.60 ± 0.63	4.40 ± 1.13	4.40 ± 1.13	3.91 ± 0.89	3.91 ± 0.89
Sequential 3 connections	0.02 ± 0.02	0.76 ± 0.18	1.28 ± 0.50	1.34 ± 0.33	2.01 ± 0.65	1.10 ± 0.32
Sequential 8 connections	0.00 ± 0.00	0.33 ± 0.07	0.02 ± 0.02	0.59 ± 0.13	1.56 ± 0.39	0.42 ± 0.07

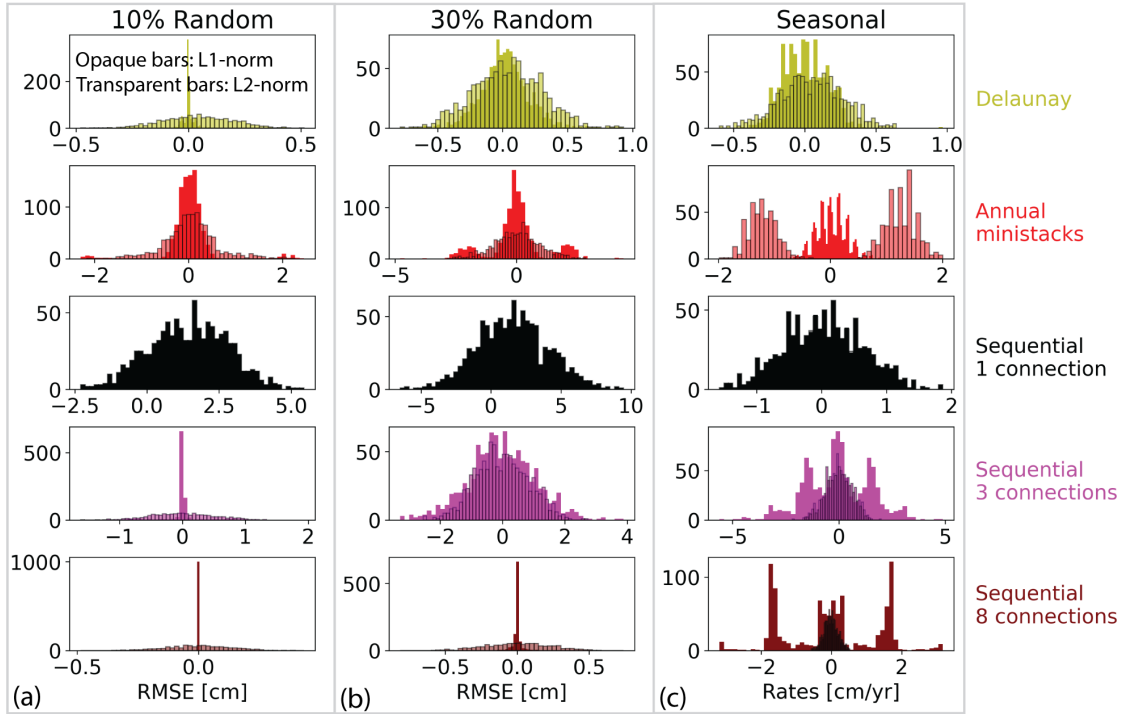


Figure S2.4: Similar to Figure S2.3 but for the velocity calculated from the estimated time series.

Table S2.2: Similar to Table S2.1 but for the velocity. Histograms shown in Figure S2.4

Unwrapping network	10% Random (cm/yr)		30% Random (cm/yr)		Seasonal (cm/yr)	
	L1	L2	L1	L2	L1	L2
Delaunay	0.00 ± 0.00	0.05 ± 0.10	0.01 ± 0.11	0.04 ± 0.18	0.00 ± 0.10	0.05 ± 0.15
Annual ministacks	0.00 ± 0.15	0.00 ± 0.29	0.01 ± 0.35	0.03 ± 0.68	0.01 ± 0.17	0.93 ± 0.73
Sequential 1 connection	1.51 ± 0.98	1.51 ± 0.98	1.53 ± 1.71	1.53 ± 1.71	0.04 ± 0.45	0.04 ± 0.45

	-0.00 ± 0.01	-0.01 ± 0.34	-0.02 ± 0.67	-0.02 ± 0.61	0.01 ± 1.15	-0.03 ± 0.43
Sequential 3 connections	-0.00 ± 0.00	-0.00 ± 0.09	-0.00 ± 0.00	-0.01 ± 0.17	-0.06 ± 1.35	0.00 ± 0.13
Sequential 8 connections	-0.00 ± 0.01	-0.01 ± 0.34	-0.02 ± 0.67	-0.02 ± 0.61	0.01 ± 1.15	-0.03 ± 0.43

S2D Unwrapping error propagation in real data

The differences of velocity maps and displacement time series obtained from the single reference network and other networks due to unwrapping error propagation for the two examples discussed in section 4.2 of the main paper are shown in Figure S2.5 and Figure S2.6.

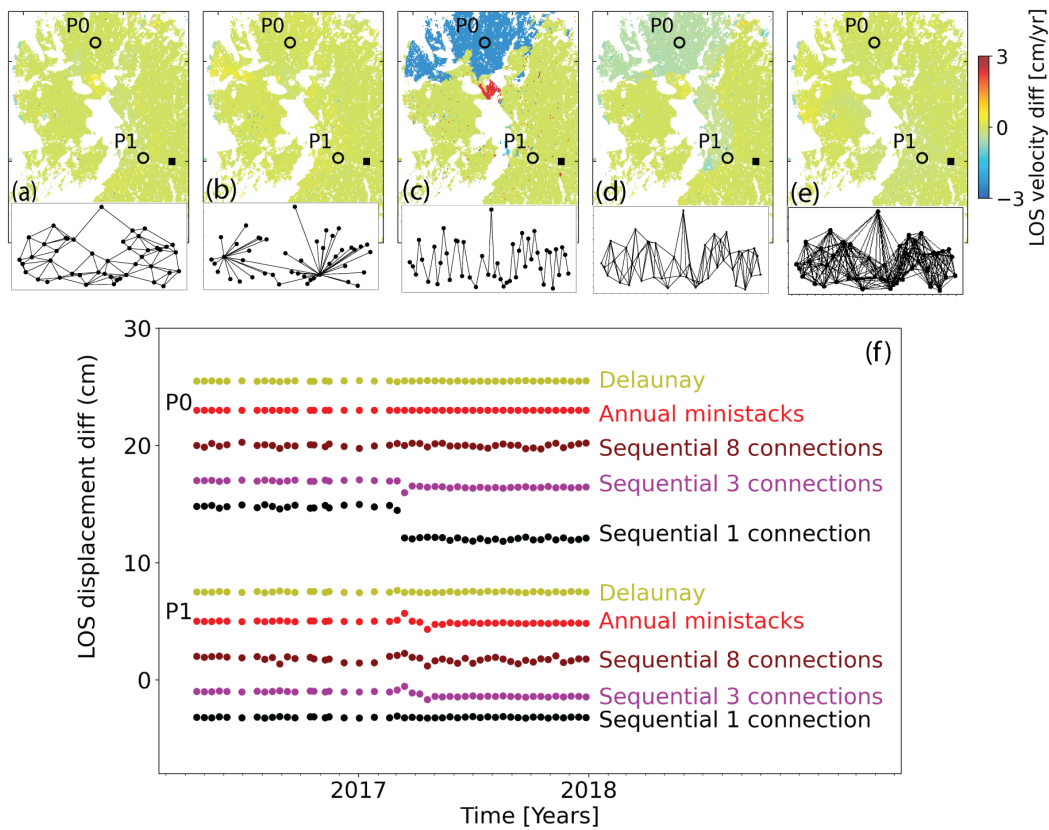


Figure S2.5: (a-e) Difference of the velocity for Guagua Pichincha (Figure 4) with respect to the single reference network for the Delaunay network, annual ministack network and sequential networks with 1, 3 and 8 connections respectively. (f) Difference in the LOS displacement time series at points P0 and P1 with respect to the time series for the single reference network for the five networks.

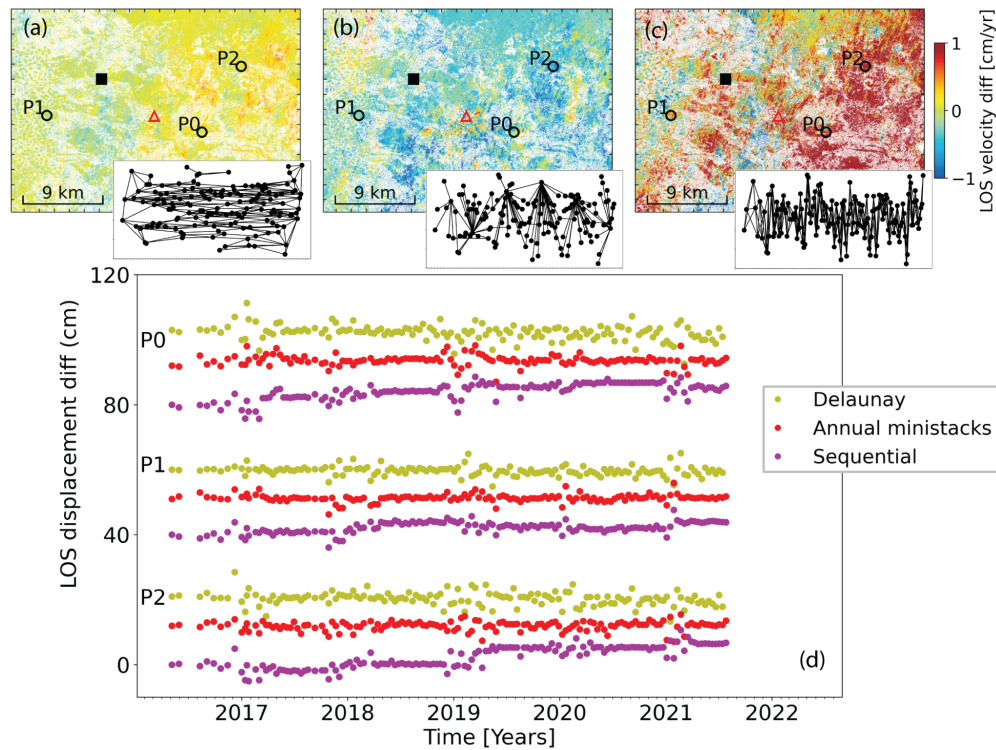


Figure S2.6: Similar to Figure S2.4 but for Mount Lassen. Refer to Figure 5 in the main paper.

Table S2.3: The RMSE of velocity difference between single reference and other networks

Unwrapping network	Delaunay (cm/y)	Annual ministacks (cm/y)	Sequential 1 connection (cm/y)	Sequential 3 connections (cm/y)	Sequential 8 connections (cm/y)
Guagua Pichincha	0.19	0.16	1.11	0.29	0.15

Mt Lassen	0.19	0.46	n/a	1.29	n/a
-----------	------	------	-----	------	-----

S2E Unwrap errors in an agricultural area (phase linking)

In this section we demonstrate for an agricultural area south of Syracuse, Sicily, Italy, that after phase linking unwrap error propagation still can lead to apparent displacements depending on the unwrapping network chosen. The area is a subset of the area studied by Ansari et al., 2021; Sentinel track 124 descending, we use 120 images from Oct 2017 to Sep 2019.

Figure S2.7a-f shows the temporal coherence of the phase linking and the velocities obtained from unwrapping five different networks, the single reference network, an annual ministack network, sequential networks with 2 and 8 connections, and a Delaunay network (pixel with temporal coherence > 0.5). The single reference network does not show any negative velocity (apparent subsidence) for the agricultural area, but the other networks do, in particular the 2-connection and 8-connection sequential networks. The negative velocities occur in areas where the temporal coherence of the phase linking is above 0.5, indicating that the phase linking could not completely fit to the model.

These results demonstrate the unwrap error propagation depending on the network described in section 4. For the single reference (Figure S2.7a) and the Delaunay networks (Figure S2.7f) a low percentage of interferograms have unwrapping error and the errors do not propagate to other acquisitions during the network inversion. In contrast, for the sequential networks (Figure S2.7d, e) in particular for 2 connections there is significant unwrap error propagation.

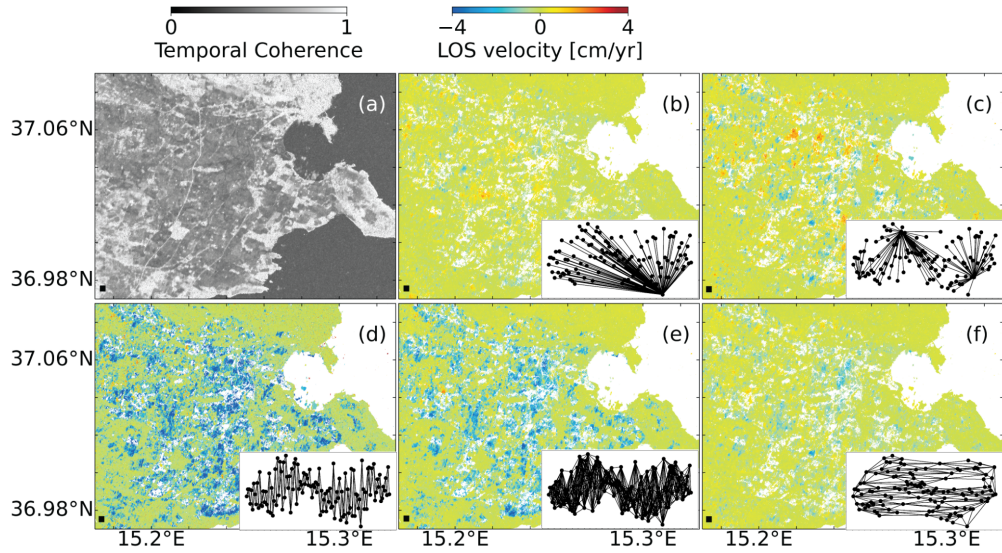


Figure S2.7: Comparison of velocities obtained from different unwrapping networks over agricultural fields.

(a) Temporal coherence of phase linking. (b) Single reference network. (c) Annual ministacks network. (d) Sequential network with 2 connections. (e) Sequential network with 8 connections. (f) Delaunay network with a scale number of 4.

S3 Additional information to section 6

The details about datasets used for different study areas is listed in Table S3.

Table S3: List of Sentinel-1 datasets used for different study areas

Study area	Acquisition period	Orbit direction and track number	Number of images	Unwrapping network	Observed temporal coherence model
Guagua Pichincha (Figure 10)	May 2016 - Jul 2021	Descending, 142	210	Single reference	Long-term decorrelated
Mount Lassen (Figure 11)	May 2016 - Jul 2021	Descending, 42	146	Single reference	Light and strong seasonal decorrelation
Three Sisters (Figure 12)	Jan 2018 - Mar 2022	Descending, 115	133	Delaunay	Strong seasonal decorrelation
Mud Creek Landslide (Figure 13)	Mar 2015 - May 2017	Descending, 42	63	Single reference	Long-term coherent
Miami Beach city	Sep 2016 -	Ascending,	143	Single reference	Long-term

(Figure 14-16)	Nov 2021	48			coherent
Bristol Dry Lake (Figure 19)	Feb 2017 - Jan 2021	Descending, 115	157	Single reference	Long-term coherent

S3A Unwrap errors versus systematic bias at Guagua Pichincha (classic small baseline)

In this section, we demonstrate that some of the signal in the classic small baseline result for Guagua Pichincha (Figure 10) is caused by phase unwrapping errors. Figure S3.1a shows the closure phase mask based on the wrapped interferograms introduced by Zheng et al (2022) which indicates regions with non-zero closure phase caused by systematic displacement bias (decaying signal). Figure S3.1b shows the number of integer non-zero closure phases for each pixel calculated from unwrapped interferograms (Yunjun et al., 2019) which indicates the regions with unwrapping errors. Given that there are only few areas with non-zero closure phase (Figure S3.1a) and there is a correlation between the pixels with high number of unwrapping errors and the pixels with LOS velocity signal (apparent subsidence in Figure 10b), the displacement bias is caused by the unwrapping error propagation and not the decaying signal.

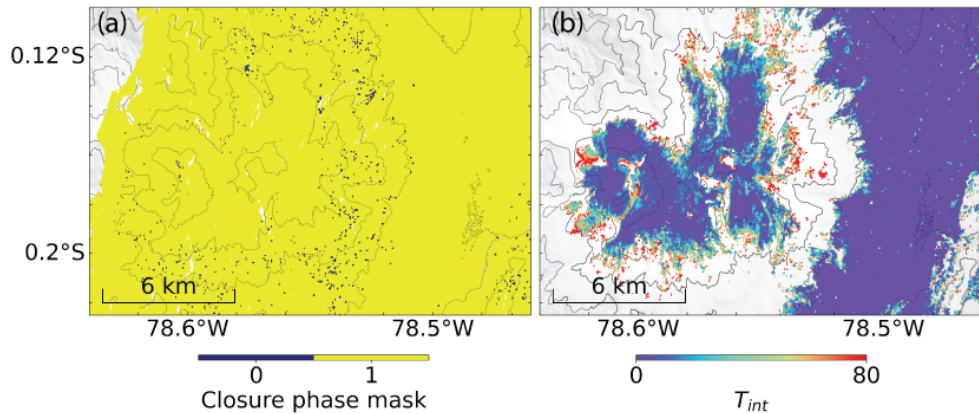


Figure S3.1: Guagua Pichincha displacement bias caused by unwrapping error. (a) Closure phase mask with zero values indicating pixels with non-zero closure phase caused by systematic bias. (b) Number of integer non-zero closure phases in the multi-looked sequential interferogram network with 4 connections (unwrapped).

S3B Small baseline unwrapping network for Mt Lassen

The network used for Mt Lassen for classic small baseline approach is a sequential network with 4 connections and annual pairs (Figure S3.2). The dashed red lines indicated the interferograms with low coherence which we remove from network inversion.

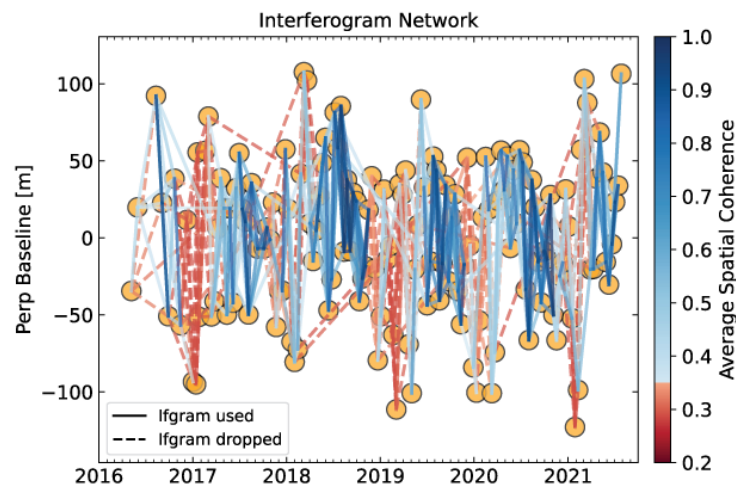


Figure S3.2: The classic small baseline unwrapping network for Mt Lassen (Figure 11b)

S3C Three Sisters LOS velocity from L2-norm minimization

In this section we show the LOS velocity maps obtained from L2-norm inversion of the Delaunay network for Three Sisters volcanoes (Figure S3.3). The inconsistencies between L1 (Figure 12b) and L2 are due to unwrapping errors in the interferograms which then impacts the displacement time series and the velocity map.

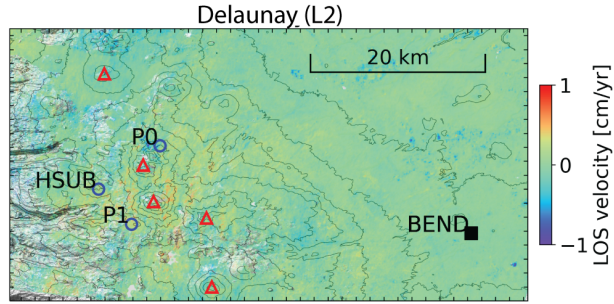


Figure S3.3: LOS velocity map from Delaunay network inversion using L2-norm minimization over Three Sisters Volcanoes. (Refer to Section 6.3 in the main paper)

S3D Subsidence on northern Miami Beach Island

The LOS velocity map of northern Miami Beach Island for the municipalities of Surfside, Bal Harbour, Bay Harbor Islands, Indian Creek are shown in Figure S3.4. The following figures show six local areas (Oceana condominium building in Bal Harbour, Figure S3.5; St Regis condominium in Bal Harbour, Figure S3.6; Kai at Bay Harbor, Figure S3.7; the Grand Beach hotel in Surfside, Figure S3.7; the Residence Inn by Marriott in Surfside, Figure S3.9 and the Surf Club hotel in Surfside, Figure S3.10 with some data repeated from Figure 15), with (a, f) the LOS velocity for the PS and DS pixel in geographic coordinates, the estimated elevation (SRTM DEM plus estimated DEM error) in (c, g) radar and (d, h) geographic coordinates, (e, f) the standard deviation of the estimated DEM error in geographic coordinates, (j) the displacement time series for selected pixels, and (k) the estimated elevation versus the digital surface model elevation.

The PS pixels on the Oceana Bal Harbour condominium building which was completed in 2016 show 1 – 4 mm/yr LOS velocity (subsidence) since 2018 (Figure S3.5), i.e., there is differential subsidence within the structure. The St. Regis condominium building in Bal Harbour which was completed in 2012 does not show any significant subsidence, but some PS and DS pixels located a few tens of meters further west show up to ~1 mm/yr LOS velocity (subsidence) (Figure S3.6). The Kai at Bay Harbor building which was completed in 2016 shows up to ~1.5 mm/yr LOS velocity (Figure S3.7). The Grand Beach hotel at Surfside which was completed in 2013 and shows ~1 – 2 mm/yr LOS velocity (Figure S3.8). The Residence Inn at Surfside was completed in 2016 and shows ~1 cm LOS displacement in 2018 and insignificant displacement after that (Figure S3.9).

Figure S3.11 shows a golf course in Indian Creek where a few isolated high temporal coherence pixels containing buildings are surrounded by low coherent pixels. The unwrapping errors of these pixels contaminate the observations for the high-coherent isolated pixels (see also Jiang and Lohman, 2021).

Figure S3.12 shows the comparison of C-band Sentinel-1 and X-band TerraSAR-X datasets over Surf Club hotel in successfully retrieving the displacement time series.

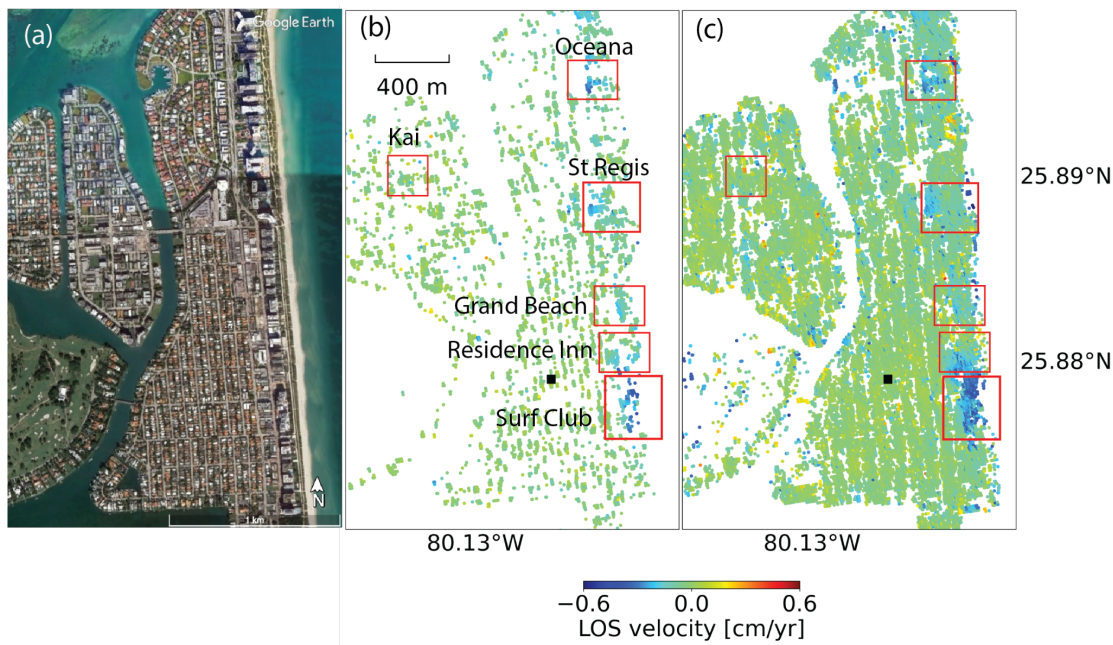


Figure S3.4: LOS velocity map for the area of northern Miami Beach Island with some of the subsiding buildings marked. (a) The optical image from Google Earth. (b) PS map. (c) Joint PS and DS map. Reference pixel is marked by black square.

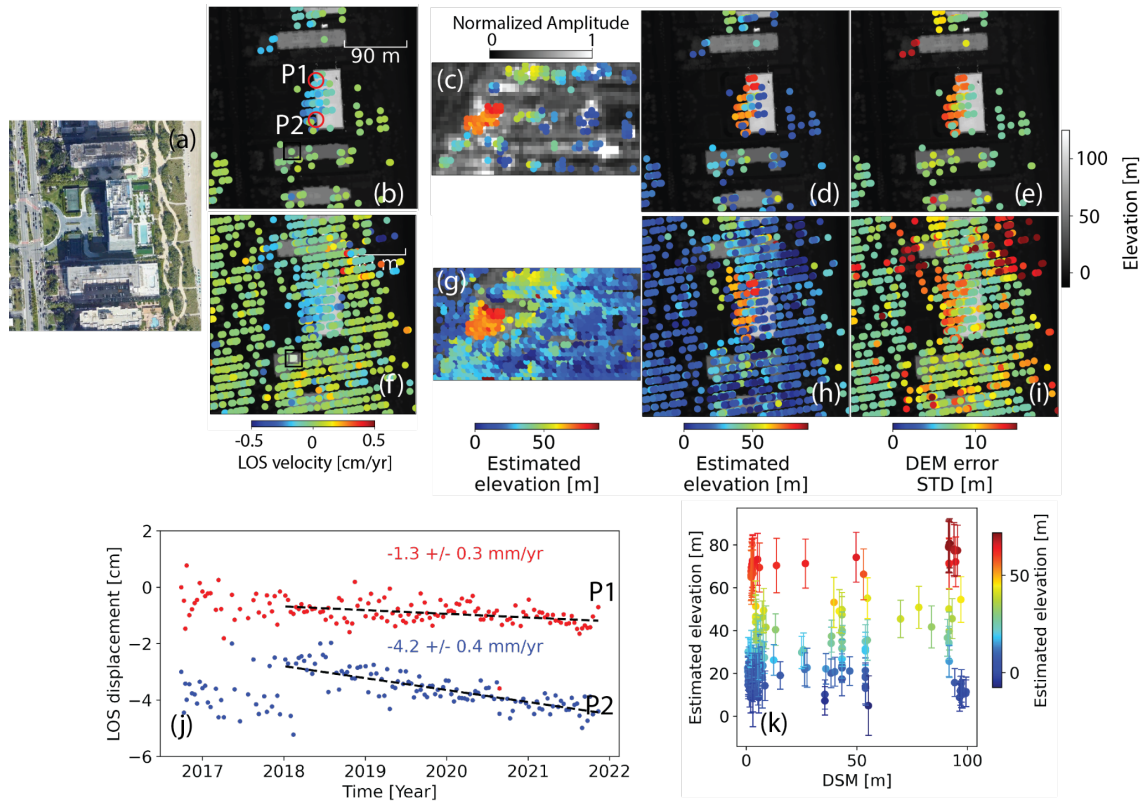


Figure S3.5: Subsidence of the Oceana Bal Harbour condominium building. (a) Google Earth optical image. (b) LOS velocity map for PS pixels superimposed on LiDAR DSM. (c) Estimated elevation in radar coordinates superimposed on radar normalized amplitude. (d) Estimated elevation in geo coordinates and (e) DEM error standard deviation superimposed on LiDAR DSM. (f-i) Same as (b-e) but for DS pixels. (j) The displacement time series for P1 and P2 (k) DSM v.s. Estimated elevation for PS pixels with bars

showing the standard deviation of DEM error and colors representing estimated elevation. Double-square in (b, f): reference point.

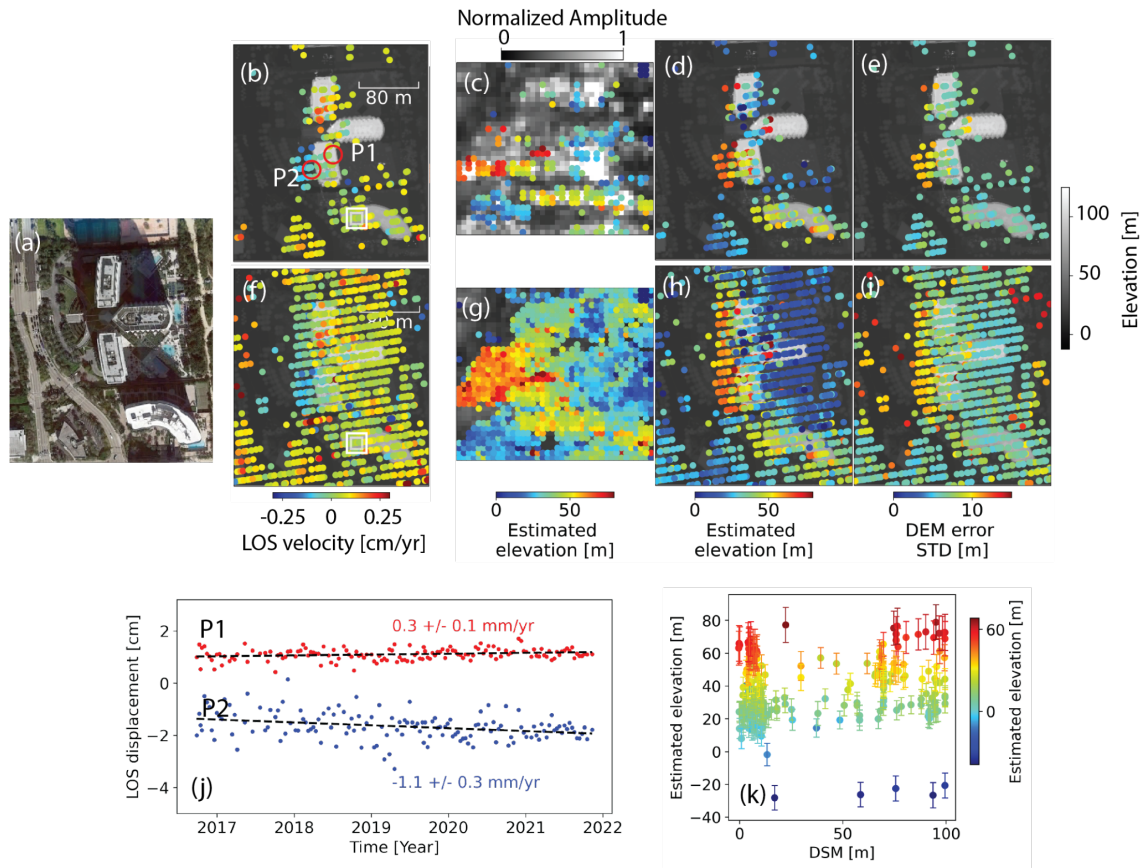


Figure S3.6: Same as Figure S3.5 but for the St Regis Bal Harbour condominium building.

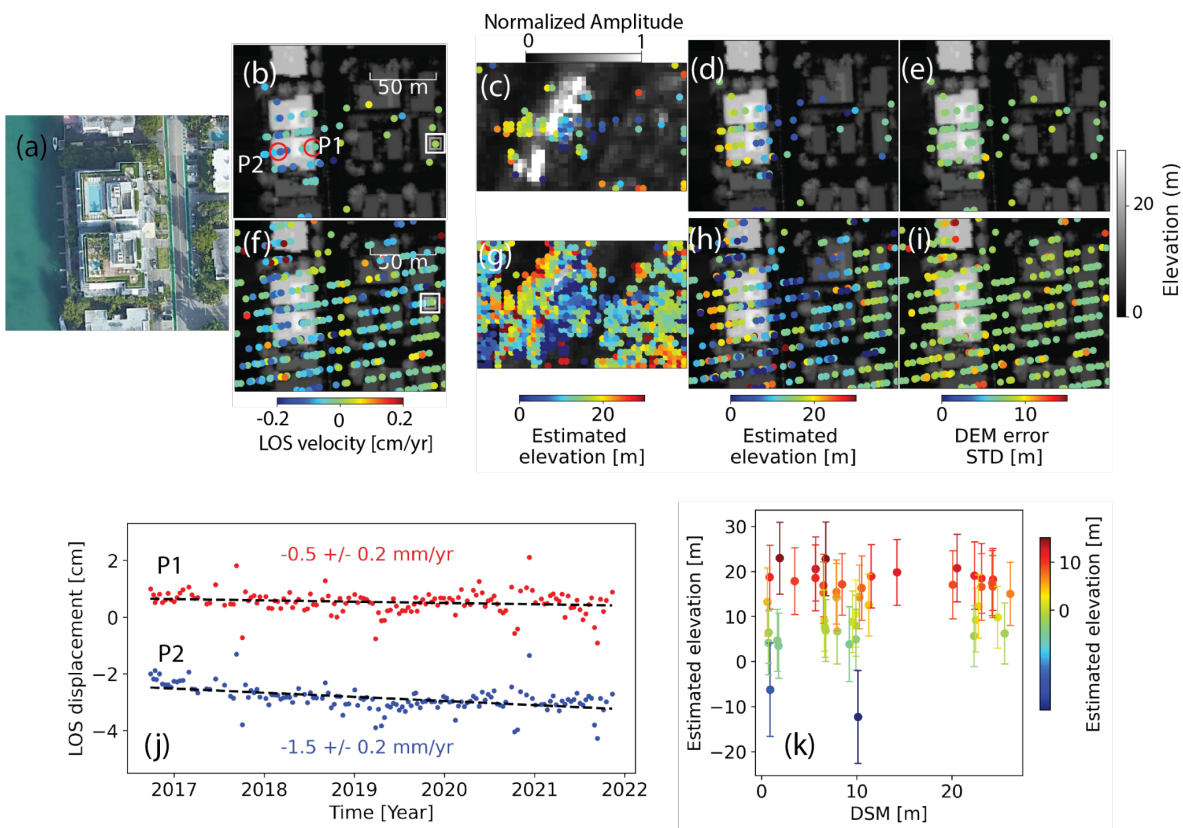


Figure S3.7: Same as Figure S3.5 but for the Kai at Bay Harbor condominium building.

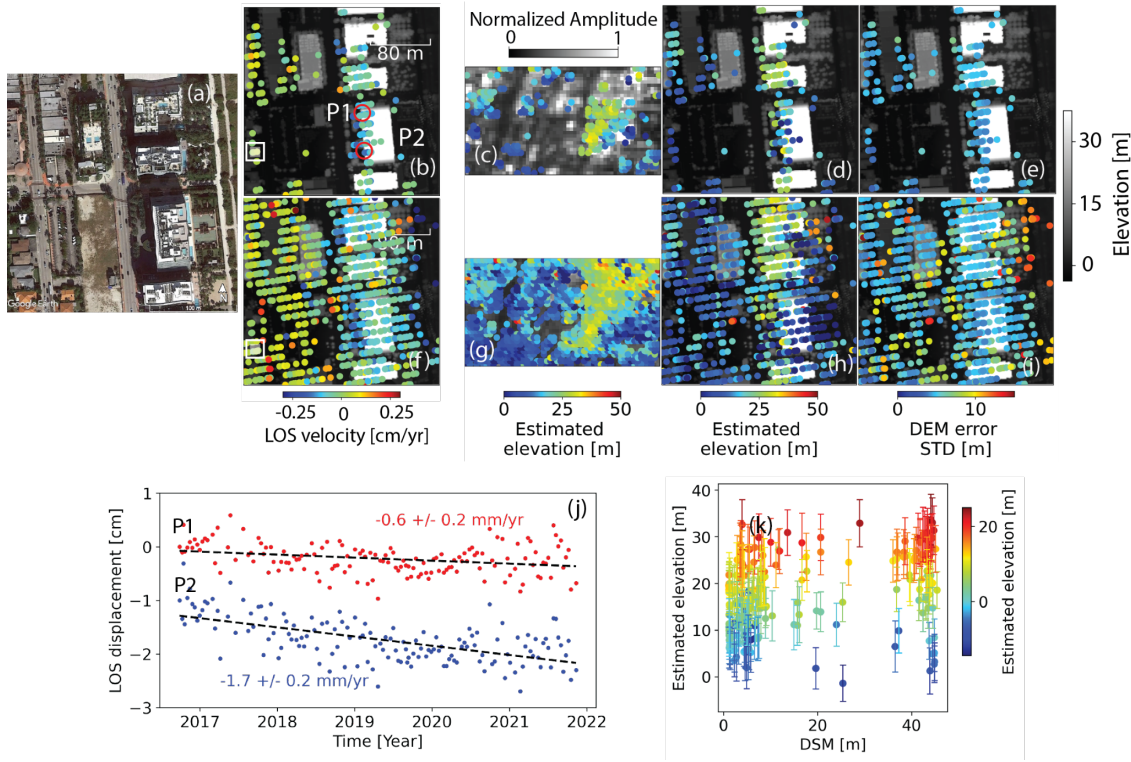


Figure S3.8: Same as Figure S3.5 but for the Grand Beach hotel building at Surfside.

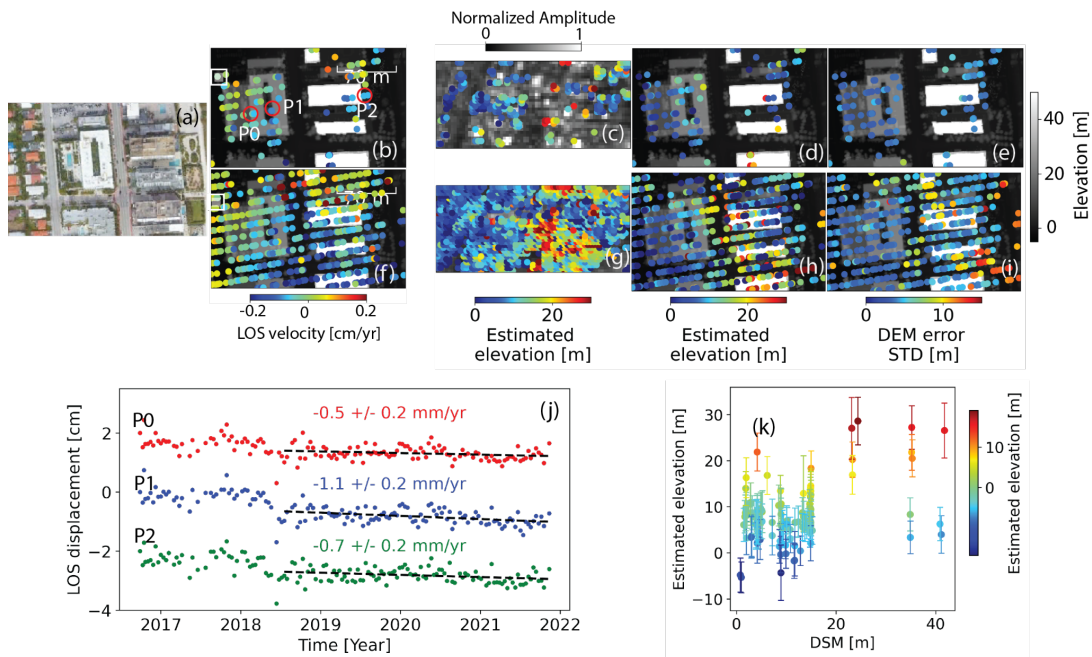


Figure S3.9: Same as Figure S3.5 but for the Residence Inn by Marriott building at Surfside.

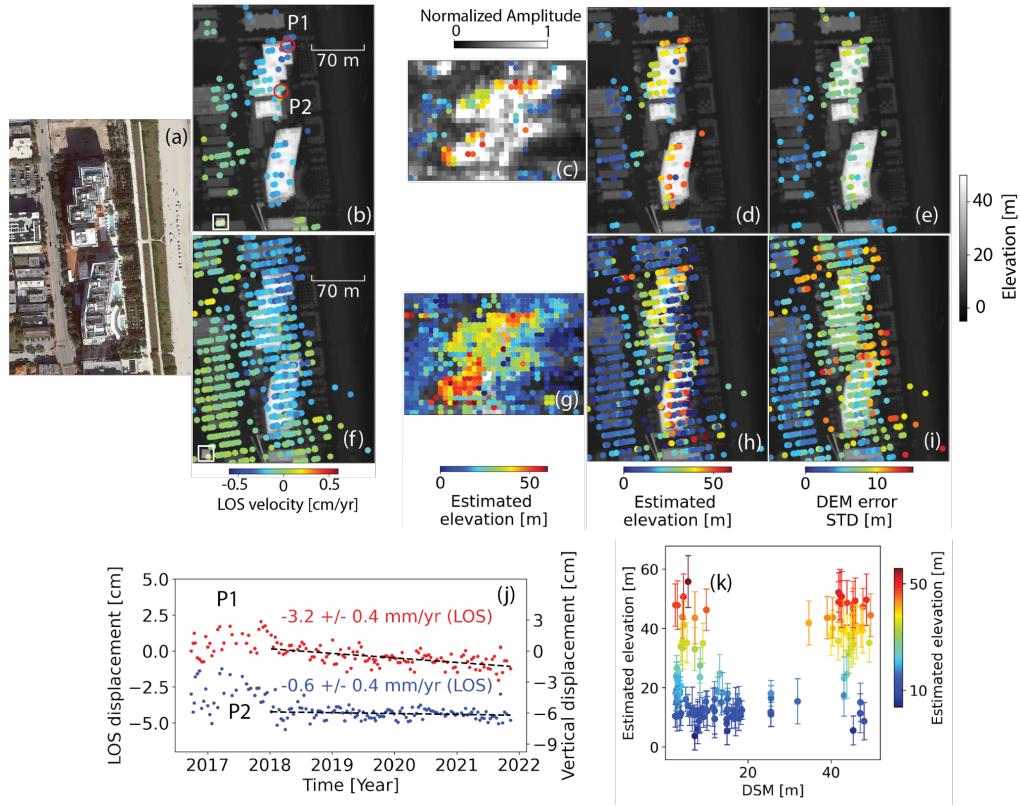


Figure S3.10: Similar to Figure S3.5 but for the Surf Club hotel in Surfside. (b, f, j) are a repeat of Figure 15b-d and (k) a repeat of Figure 16e but include the uncertainties of the estimated elevations.

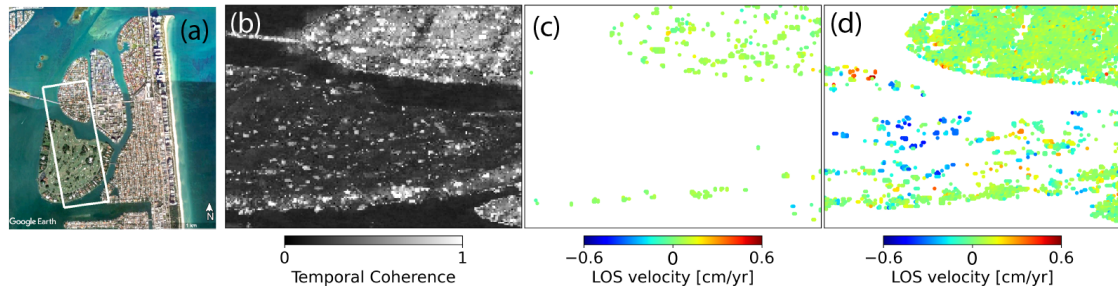


Figure S3.11: Isolated PS and DS pixels showing limitations of phase unwrapping. (a) Google Earth optical image. (b) Temporal coherence from phase linking. (c) PS pixels and (d) DS pixels.

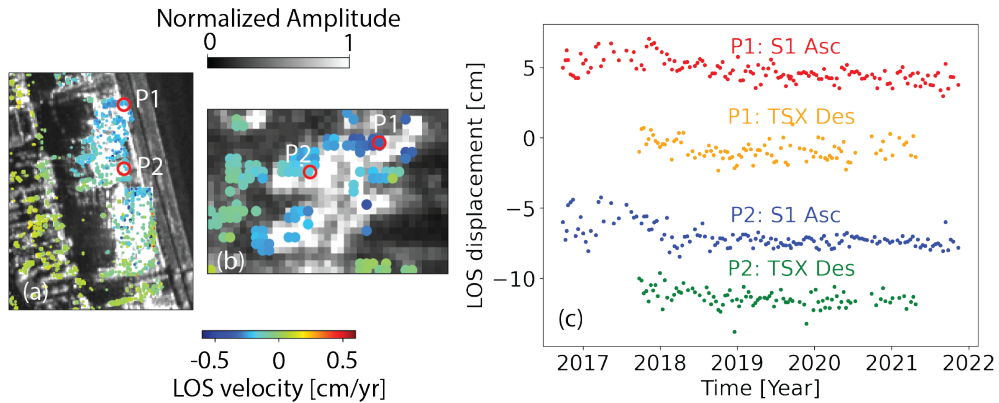


Figure S3.12: Comparison of TerraSAR-X and Sentinel-1 results on the Surf Club hotel subset.(a) Velocity map obtained from TerraSAR-X descending dataset (Sep 2017-Apr 2021). (b) Velocity map obtained from Sentinel-1 ascending dataset (Sep 2016-Nov 2021). (c) Timeseries of points P1 and P2 comparing TerraSAR-X and Sentinel-1.

S4. Technical software guide

The program language is Python and it has a size of 199 KB. The hardware requirements include a physical server or virtual machine with a CPU of 2 x 64-bit, 2.8 GHz, 8.00 GT/s or better. It requires a minimum RAM size of 32 GB, or 16 GB RAM with 1600 MHz DDR3 installed. The required software is a client environment including Linux, macOS or Windows and Python libraries and tools listed in the [installation guide](#).

Customizable parameters are initiated in a configuration text file with default values ([link on GitHub](#)).The subset area can be given by latitude, longitude extent or radar coordinate extent and a file containing the cropped SLCs is created. Parameters for each step can be modified in the configuration text file. For the phase linking step, the number of parallel processors can be defined based on the computing resources available to speed up. If a MiaplPy step stops for any reason, it will continue processing from where it stopped by rerunning that step. The phase linking is implemented in Cython and requires compiling to install the software properly. Instructions can be found on [GitHub](#).

MiplPy outputs and steps are adapted to work with the MintPy software, and all corrections can be applied using MintPy. Most of the scripts are standalone and users can call them separately or using the routine workflow with step names (Instructions on GitHub).

Table S4: Stand-alone scripts in MiaplPy

correct_geolocation.py	Correct for geolocation offset caused by DEM error
generate_ifgram.py	Generates interferograms from wrapped phase series based on the selected network
generate_coherence_mask.py	Generates temporal coherence map from phase linking results
load_ifgrams.py	Loads the unwrapped interferograms into a stack with hdf5 format (ifgramStack.h5)
load_slc_geometry.py	Loads the input data into stacks of hdf5 format (slcStack.h5 and geometryRadar.h5)
miaplpyApp.py	Routine workflow of MiaplPy
network_inversion.py	Inverts the unwrapped network of interferograms for displacement time series
phase_linking.py	Performs the phase linking in parallel by dividing data into patches and then concatenates the patches
prep_slc_isce.py	Prepares metadata for input data
simulation.py	Phase linking simulation and assessment
tcoh_view.py	A wrapper to interactively display time series and the corresponding coherence matrix for each pixel
unwrap_ifgram.py	Unwraps the selected network of interferograms

S4A. Computational considerations

In this section, we first provide a benchmark for the processing time of one pixel and then describe how large areas can be analyzed with parallel processing. The steps requiring computational resources are the phase linking and the subsequent interferogram unwrapping.

S4A.1 Phase linking of one pixel

The average time for phase linking of one pixel with 100 acquisitions after 1000 realizations on a 2.8 GHz Quad-Core Intel Core i7 processor is shown for each method in Figure S4a. For the long-term decorrelated model (green bars), the eigenvalue-based maximum likelihood approach is the fastest (~ 14 milliseconds compared to ~ 35 milliseconds for classic eigenvalue decomposition). For the long-term coherent signal (pink bars), the classic eigen value decomposition and the eigenvalue-based maximum likelihood approaches require similar time for convergence (~ 13 milliseconds). The sequential modes take $\sim 30\%$ of the processing time of the non-sequential modes and outperform all methods with sequential classic eigenvalue decomposition slightly faster than sequential eigenvalue-based maximum likelihood. The processing time increases exponentially with more images (Figure S4b) for methods with regular implication with different rates, however, turns out to be more linear for sequential mode with a rate of ~ 0.2 milliseconds per image.

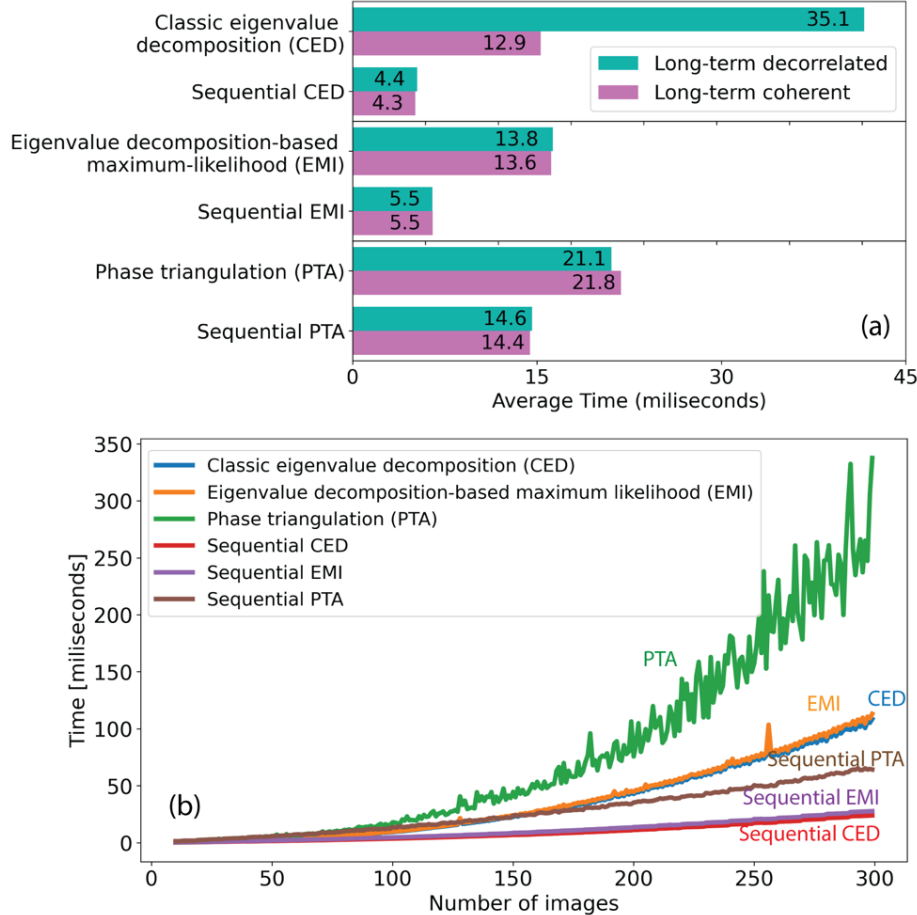


Figure S4: Timing the phase linking methods. (a) Average processing time for one pixel for each method in regular implication mode and sequential mode. Green bar refers to the long-term decorrelated scenario while pink refers to long-term coherent scenario. (b) Time increases as a function of the number of images

S4A.2 Phase linking of an area using parallel processing

Assuming a time of 4.6 milliseconds for phase linking of one pixel of 100 images using the sequential eigenvalue-based maximum likelihood algorithm (ministack size of 10), a simple calculation shows that an area of 1000×1000 pixels would take ~ 77 minutes. To speed up this process, the area is split into patches which are processed simultaneously. The processing of one patch with default size of 200×200 pixels take 184 seconds (~ 3 minutes). If 25 cores are available, the entire area can be processed during this time. Of

course, additional images increase the processing time. On high performance computers with N nodes (processors), each with n cores, a total of $N \times n$ patches can be processed simultaneously.

Supplemental references

- Ansari, H., De Zan, F., Parizzi, A., 2021. Study of Systematic Bias in Measuring Surface Deformation With SAR Interferometry. *IEEE Trans. Geosci. Remote Sens.* 59, 1285–1301.
<https://doi.org/10.1109/TGRS.2020.3003421>
- Jiang, J., Lohman, R.B., 2021. Coherence-guided InSAR deformation analysis in the presence of ongoing land surface changes in the Imperial Valley, California. *Remote Sens. Environ.* 253, 112160. <https://doi.org/10.1016/j.rse.2020.112160>
- Yunjun, Z., Fattah, H., Amelung, F., 2019. Small baseline InSAR time series analysis: Unwrapping error correction and noise reduction. *Comput. Geosci.* 133, 104331.
<https://doi.org/10.1016/j.cageo.2019.104331>
- Zheng, Y., Fattah, H., Agram, P., Simons, M., Rosen, P., 2022. On Closure Phase and Systematic Bias in Multi-looked SAR Interferometry. *IEEE Trans. Geosci. Remote Sens.* 60, 1–1.
<https://doi.org/10.1109/tgrs.2022.3167648>